Bistable transport properties of a quasi-one-dimensional Wigner solid on liquid helium under continuous driving

David G. Rees,[1,2,3,*] Sheng-Shiuan Yeh,[1] Ban-Chen Lee,[1] Kimitoshi Kono,[1,2,3] and Juhn-Jong Lin[1,2,4]

[1]*NCTU-RIKEN Joint Research Laboratory, Institute of Physics, National Chiao Tung University, Hsinchu 300, Taiwan*
[2]*RIKEN CEMS, Wako 351-0198, Japan*
[3]*KFU-RIKEN Joint Research Laboratory, Institute of Physics, Kazan Federal University, Kazan 420008, Russia*
[4]*Department of Electrophysics, National Chiao Tung University, Hsinchu 300, Taiwan*

We investigate low-frequency fluctuations in the transport characteristics of a quasi-1D Wigner solid (WS) moving along a liquid helium substrate in response to a sinusoidal driving voltage. The fluctuations occur between distinct transport modes in which the decoupling of the WS from ripplonic polarons (or "dimple lattice," DL) formed on the helium surface does, or does not, occur during each ac cycle. We demonstrate that a Gaussian-like distribution in the decoupling threshold force gives rise to this bistability, as the low-frequency switching occurs when the probability of decoupling during each ac cycle is small but finite. We attribute the distribution in the decoupling threshold force to the range of structural configurations allowed for the quasi-1D electron lattice, which influences the strength of the WS-DL coupling. Hence, the switching rate between the ac transport modes is extremely sensitive to the microscopic properties of the electron solid.

I. INTRODUCTION

Bistable behavior has been studied extensively both experimentally and theoretically in a wide variety of physical systems including electromechanical resonators [1,2], Josephson junctions [3], and trapped electrons and atoms [4,5]. Bistability can also be induced or triggered in dynamical systems by parametric driving [6–9]. Here we demonstrate a bistable process observed in the transport of electron crystals trapped on the surface of liquid helium and driven back and forth through a narrow channel. Transport modes in which the electrons are coupled to or decoupled from helium surface excitations provide two "states" between which a stochastic switching can occur. We demonstrate that this effect arises due to a distribution in threshold force at which the electron crystal decouples from the helium surface. As well as revealing information regarding the interaction between the electron crystal and its liquid substrate, our experiment provides a clear example of how the application of a continuous driving force can invoke and elucidate metastability in dynamical systems.

At sufficiently low temperatures, electrons trapped on the surface of liquid helium [10,11] self-organize to form a triangular lattice, the Wigner solid (WS) [12,13]. Unlike the WS states found in degenerate 2D electron systems in the quantum regime [14], the WS on helium is essentially classical in nature due to the relatively low electron densities ($10^9 \lesssim n_s \lesssim 10^{13}$ m^{-2}) that can be supported by the helium substrate. In addition, the Coulomb interaction between the electrons is not screened by the helium, which has a permittivity close to that of vacuum. This makes surface electrons an ideal model system for the study of strongly correlated electron behaviors in 2D [15] and, in recent experiments using microchannel devices [16], transport at the nanoscale in the limit of strong electron-electron interaction [17,18].

The interaction between the electron lattice and the liquid-vacuum interface gives rise to several intriguing phenomena. The pressure exerted on the helium surface by each electron results in a shallow deformation of the liquid, beneath each electron, which is known as a "dimple" [19,20]. Equivalently, and in analogy with polaron states formed by electrons coupled to virtual phonons in crystal lattices, the static electron solid can be described as being "dressed" by quantized capillary waves (ripplons) [21,22]. Because the combined mass of the electron and its dimple is much greater than the bare electron mass, the conductance of the electron system usually drops dramatically when the system enters the solid phase [23]. However, the electron system can be decoupled from the surface deformation by the application of a strong electric field parallel to the helium surface [24]. After decoupling, the WS can move freely across the helium with high velocity. Analogous decoupling processes occur for polarons formed in solid-state systems [25].

In recent time-resolved transport measurements, a repeated decoupling of the Wigner solid from the dimple lattice (DL) was observed for a WS moving through a helium-filled microchannel a few microns in width, in response to a smoothly ramped driving voltage [26]. The consequent "stick-slip" motion of the electron system resulted in spontaneous current oscillations, the frequency of which was dependent on the strength of coupling between the WS and the helium substrate and on the applied driving force. However, many details regarding the decoupling process remain poorly understood. In this report we present transport measurements that uncover important information regarding the WS-DL decoupling. We demonstrate that during a driving voltage ramp, the threshold electric field at which the decoupling can occur follows a Gaussian-like distribution. We then investigate the influence of this threshold distribution on the WS response to a sinusoidal driving voltage. In this case, two transport modes are possible; in the first mode the WS-DL decoupling occurs once during each half of the ac cycle, while in the second mode the WS and DL always remain coupled. Because, under continuous
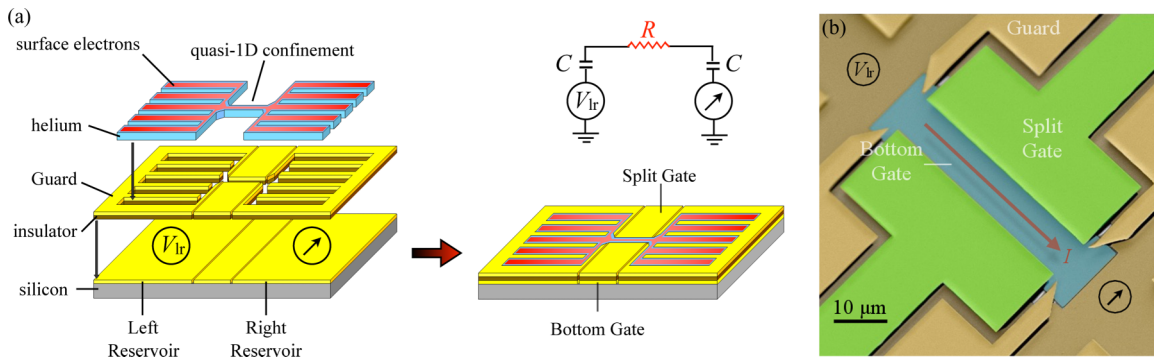
FIG. 1. (a) Schematic picture of the microchannel device. The left- and right-reservoir and bottom-gate electrodes in the lower layer are separated from the guard and split-gate electrodes in the upper layer by hard-baked photoresist. Liquid helium fills the channel structures by capillary action. Electrons are then deposited on the helium surface. The device can be represented by the simplified RC circuit diagram. (b) False-color scanning electron micrograph of the device. The surface electron current I flows through the central microchannel in response to the driving voltage V_{lr} and induces a displacement current in the right-reservoir electrode.

driving, the response during one cycle influences the behavior during the next, the system can become "locked" in one mode or the other. However, the distribution in the decoupling threshold force allows the system to occasionally "switch" between the modes, resulting in telegraph-like "noise" in the current amplitude. By tuning the system into a regime in which these fluctuations are rare, the average time between switching events becomes much longer than the ac driving period. The low-frequency noise observed in our experiment can reveal information regarding the microscopic details of the quasi-1D electron crystal.

The paper is arranged as follows. In Sec. II we describe the sample and experimental setup. In Sec. III we present experimental evidence of the distribution in the WS-DL decoupling force threshold. In Sec. IV we demonstrate that, close to the decoupling point, a bistable conductance regime can be realized by applying a sinusoidal drive to the electron system. In Sec. V we discuss the origin of this bistability, demonstrating the link between the low-frequency current fluctuations and the decoupling threshold distribution. In Sec. VI we give details of further measurements in which the dependence of the bistable behavior on both temperature and the commensurability of the electron lattice within the microchannel confinement was investigated. In Sec. VII we make our conclusions. A glossary of the abbreviated terms used in the text is given in the Appendix.

II. EXPERIMENTAL

The sample, which is shown in Fig. 1, and the measurement setup used in the experiments have been described in detail elsewhere [27,28]. The sample is fabricated using UV lithography on a section of silicon wafer. Two gold layers, separated by a 2.2-μm-thick layer of insulating hard-baked photoresist, are patterned to form the various electrodes that are used to confine and manipulate the electron system. In the upper layer, the guard electrode forms the perimeter of the sample and defines two arrays of microchannels, in which each microchannel is 20 μm wide, that are used to store a large number ($\sim 10^6$) of electrons. These regions are denoted the left and right reservoirs. A small central microchannel connects the two reservoirs; its geometry is defined by the split-gate electrode.

The central microchannel is 7.5 μm wide and 100 μm long. In the lower metal layer, the bottom-gate electrode covers the area at the bottom of the central microchannel, and the left- and right-reservoir electrodes cover the area at the bottom of the left and right reservoirs, respectively. The microchannels are filled by the capillary action of superfluid helium when the liquid surface is close to the sample. Surface electrons are then generated by thermionic emission from a tungsten filament situated a few mm above the sample.

To trap electrons in the reservoirs and to control their transport through the central microchannel, dc voltages $V_{gu} = -0.2$ V, V_{sg}, and V_{bg} were applied to the guard, split-gate, and bottom-gate electrodes, respectively. Transport measurements were made by applying ramped or sinusoidal driving voltages to the left-reservoir electrode using an arbitrary wave form generator; the time-dependent voltage on the left reservoir is denoted V_{lr}. The displacement current induced in the right-reservoir electrode (which is held at dc ground) was then measured using a current preamplifier and either a lock-in amplifier or a digital storage oscilloscope. For the time-resolved measurements of current fluctuations, the demodulated signal from the lock-in amplifier was monitored using a spectrum analyzer. All measurements were made at temperature $T = 0.6$ K, unless otherwise stated.

III. RESPONSE TO A VOLTAGE RAMP

We start by analyzing the response of the quasi-1D WS to a smooth voltage ramp. In Fig. 2(a) we show the surface electron current I that flows in response to a change in V_{lr} from 0 to +50 mV in 80 μs. Here $V_{sg} = -1$ V and $V_{bg} = 1.14$ V. According to finite-element modeling (FEM) [27,29], under these bias conditions the effective width of the quasi-1D electron system is $w_e = 4.0$ μm, $n_s = 2.3 \times 10^{13}$ m^{-2}, and the electron lattice comprises approximately 18 electron rows. The current was measured using a preamplifier (Femto DHPCA-100) with wide bandwidth (3.5 MHz). To resolve the signal above the experimental noise, the signal was averaged some 8000 times.

Two current peaks are recorded as V_{lr} increases, due to the repeated decoupling of the electron system from the dimple lattice. The period separating the decoupling events, and the
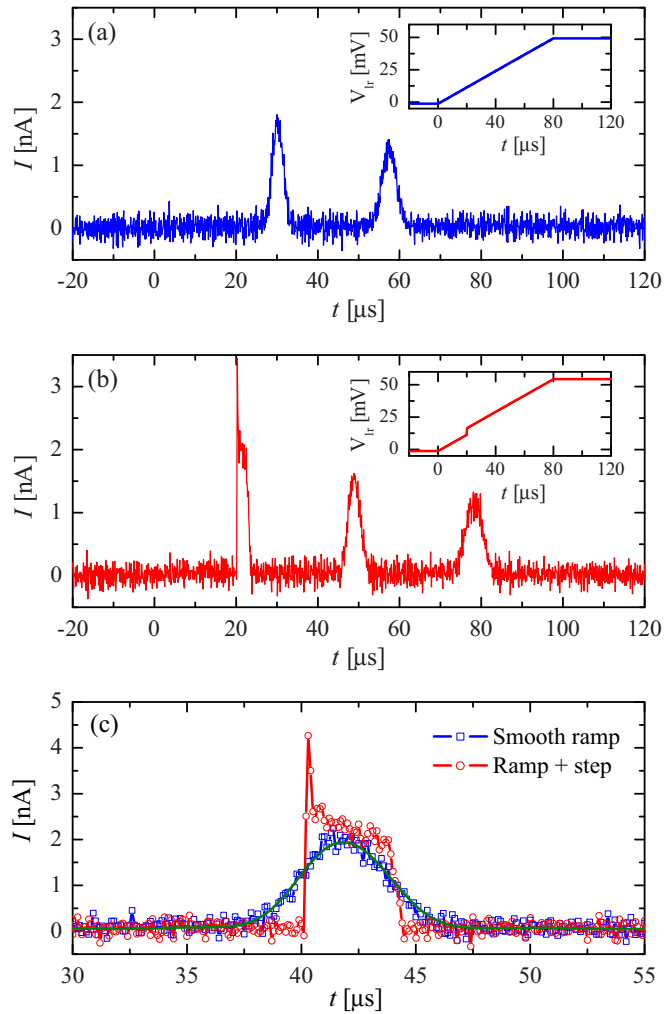
FIG. 2. (a) I against t for a smooth V_{lr} ramp from 0 to $+50$ mV in 80 μs, as shown in the inset. Here $V_{sg} = -1$ V and $V_{bg} = 1.14$ V. (b) I against t for the same conditions but with the addition of a step of $+5$ mV to the V_{lr} ramp at $t = 20$ μs, as shown in the inset. (c) I against t for a smooth V_{lr} ramp recorded for $V_{bg} = 1.3$ V (squares). For this condition the current peak appears after approximately 50 μs. However, in the plot the data are shifted by -9.2 μs in order to allow comparison with the current recorded when a $+5$ mV voltage step is added to the V_{lr} ramp at $t = 40$ μs (circles). The solid line shows the result of simulating the effect of a Gaussian distribution in the WS-DL decoupling threshold, as described in the text.

shape of the resulting current peaks, is consistent with previous measurements [26]. The decoupling occurs due to the building of the driving electric field E_x that acts on the electron system when V_{lr} is ramped. At the beginning of the ramping phase, the WS moves with the DL. As the velocity of the system approaches the phase velocity v_r of ripplons whose wave vector matches the first reciprocal lattice vector of the electron lattice, the moving electrons excite ripplons which interfere constructively with the dimple lattice. As a result, the dimples become deeper and the drag force acting on the WS increases. The Wigner solid therefore becomes dynamically pinned to the dimple lattice, at velocity v_r [30]. This process is known as Bragg-Cherenkov (BC) scattering [31]. Because the resonant ripplon wave vector is well defined (by the periodicity of the

electron lattice) this velocity can be readily determined from the ripplon dispersion relation, if the electron density is known. The ripplon dispersion relation is $\omega^2 = (\alpha/\rho)k^3$ where ω is the ripplon angular frequency, α is the helium surface tension, ρ is the liquid density, and k is the ripplon wave vector that, under the BC resonance, is equal to the first reciprocal lattice vector of the electron solid G_1. (We do not consider the correction to the dispersion relation due to the presence of charges above the helium surface, as this results in a change in ω of less than 1%, for the range of wave vectors involved in the BC scattering [32]). For the conditions in Fig. 2 the velocity at which the BC resonance occurs is $v_r = \omega/G_1 = 8.2$ m s^{-1}, which results in a current $I_{BC} = e n_s w_e v_r = 100$ pA (close to the noise floor of the measurement). However, in the limit of zero electrical resistance the WS would travel at a greater velocity, as determined by the V_{lr} ramp rate, the capacitance of the electron sheet to the reservoirs $C = 1.0$ pF, w_e, and n_s; we estimate this velocity to be 23.3 m s^{-1}. Hence the reduced velocity of the coupled WS-DL system leads to the increase in E_x as V_{lr} is ramped. As E_x grows, a threshold value of E_x is eventually reached at which the WS decouples from the DL, and the electrons move across the helium surface at a velocity much higher than v_r. The resulting burst of current largely restores the electrostatic equilibrium, and the driving field is reduced. The WS can then recouple with the DL and the stick-slip cycle can start again.

The distinct current oscillations due to the stick-slip WS motion have been described previously [26]. However, because signal averaging was necessary to resolve the current above the background noise, it was not certain that this measurement recorded the true dynamics of an individual decoupling event. To investigate this issue, the measurement shown in Fig. 2(a) was modified by adding a small voltage step of $+5$ mV (made in 0.1 μs) to the usual smooth voltage ramp, at $t = 20$ μs [just before the first current peak appears in Fig. 2(a)]. This voltage step is large enough to increase the driving force (which already approaches the threshold value during the smooth section of the voltage ramp) above that required for decoupling to occur. The response to the modified ramp is shown in Fig. 2(b). A current peak now appears at $t = 20$ μs, with a quite different line shape from those in Fig. 2(a). The current rises abruptly and then flows at an almost constant value, before decreasing rapidly again. Following this, two subsequent decoupling events occur, which generate current peaks similar to those observed in Fig. 2(a).

The addition of a sharp voltage step to the smooth ramp (before, but close to, the point at which the WS decouples from the DL during the smooth voltage ramp) ensures that the WS-DL decoupling is induced within the 0.1 μs step for each driving voltage cycle. In this case, although averaging is still used to resolve the current signal, the measured increase in the current at $t = 20$ μs is extremely sharp; it follows that the current peaks observed when no voltage step is applied appear smooth due to an averaging of many decoupling events that each occur at slightly different times. To test this hypothesis, we assume that the distribution of the decoupling times is Gaussian in nature and described by a standard deviation σ_t. In Fig. 2(c) we take a typical example of the current signal synchronized by the small voltage step (in this case at $t = 40$ μs) and simulate the effect of averaging many of

these signals with a distribution in their decoupling times. For each data point, recorded at time t_p, we generate a Gaussian distribution centered about t_p, the sum of which has an amplitude equal to the value of that data point. We then sum these distributions. As shown in Fig. 2(c), the result is a smooth current peak that, for $\sigma_t = 1.4$ μs, closely matches a typical example of a current peak recorded during the smooth voltage ramp (these data are shifted by -9.2 μs to allow comparison). We conclude that a Gaussian-like distribution in the times at which the WS decouples from the DL accounts for the smoothed appearance of the stick-slip current features. The unusual current flow in response to the voltage step, with a plateau-like feature at an electron velocity much greater than v_r, indicates that the interaction between the electrons and the helium substrate remains highly nonlinear even in the decoupled state. The plateau feature does not depend on the voltage step size. However, the complex interaction between the electrons and the helium in this regime goes beyond the scope of this report and will be examined in more detail elsewhere.

The observation that the WS-DL decoupling occurs in a stochastic manner also explains the reduced amplitude of the second current peak in Fig. 2(a). Because the second decoupling events depend on the time at which the first occur, but also follow the same Gaussian-like distribution, the second peak appears more smoothed than the first. As expected, subsequent peaks become further broadened [26].

The stochastic nature of the WS-DL decoupling under a ramped potential indicates that the driving electric field at which the electron system decouples from the DL is not the same on each voltage cycle. For the measurement shown in Fig. 2(a), the rate of change of voltage across the electron system, before the decoupling occurs, is $dV_{lr}/dt - 2I_{BC}/C \approx 445$ V s^{-1}. The value of σ_t can be used to characterize the distribution in driving voltage (and electric field) at which the decoupling occurs; $\sigma_t = 1.4$ μs corresponds to a standard deviation in the voltage and electric field threshold distribution of $\sigma_V = 0.62$ mV and $\sigma_{E_x} = 6.2$ V/m, respectively.

IV. RESPONSE TO A SINUSOIDAL VOLTAGE

The distribution of the WS-DL decoupling threshold has an important consequence when the WS is driven continuously by a sinusoidal voltage, namely the appearance of a bistability in the surface electron conduction. In Fig. 3(a) we show examples of the surface electron current that flows in response to a sinusoidal driving voltage of frequency 20.2 kHz and amplitude 40 mV (peak-to-peak) for two values of V_{bg}. Here $V_{sg} = -0.5$ V. In this measurement we employ a current preamplifier (Stanford Research SR570) with low noise characteristics but a reduced bandwidth (200 kHz). Signal averaging over several thousand cycles is again employed to resolve the (average) current. For the lower value of V_{bg}, a current peak is observed during each ac half cycle as the WS decouples from (and then quickly recouples to) the DL. For the higher value of V_{bg}, the electron density and the pressing electric field perpendicular to the helium surface are increased and no decoupling occurs. For $V_{bg} = 1.43$ V, we calculate $I_{BC} = 0.264$ nA, which is in close agreement with the current plateaus observed for the coupled WS-DL system [30]. By integrating the current
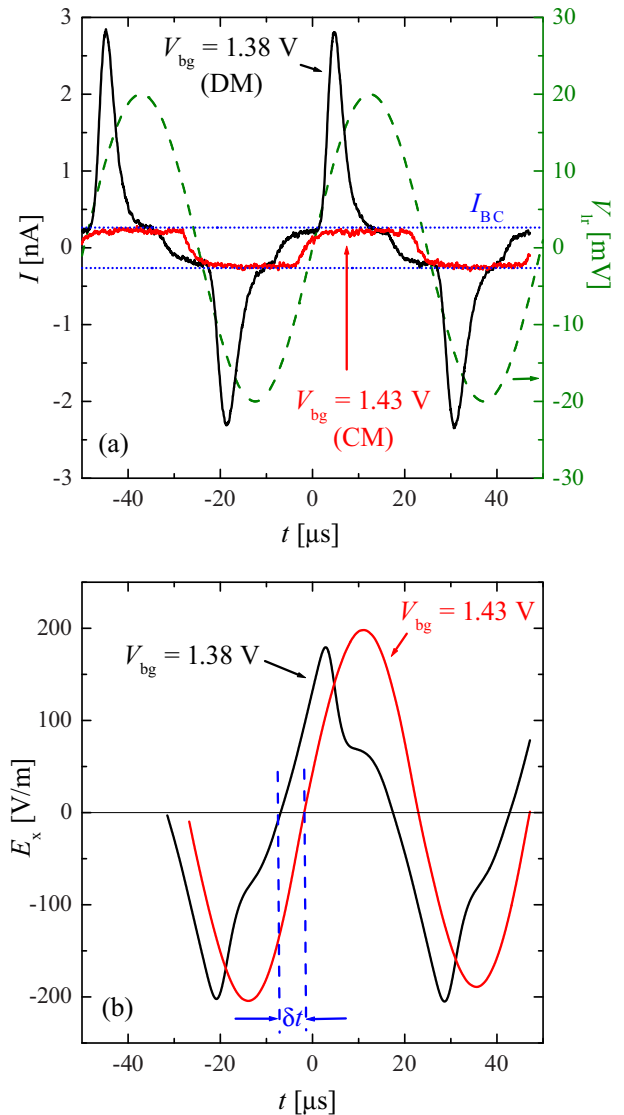

FIG. 3. (a) I recorded for the decoupled mode (DM) and the coupled mode (CM) (solid lines) and the sinusoidal driving voltage V_{lr} (dashed line), plotted against t. The dotted lines show the value of I_{BC} for electron motion in both directions along the channel. Here $V_{sg} = -0.5$ V. (b) The variation of E_x against t for the DM and CM data shown in (a). The phase difference between the two signals δt is defined as the difference in the times at which E_x becomes zero in the two conductance modes, as described in the text.

signal, the number of electrons that pass through the central microchannel, and so the voltage drop due to this current flow, can be calculated. This voltage is subtracted from V_{lr} in order to determine E_x at each value of t. This is shown in Fig. 3(b). It is clear that the decoupling of the WS results in a drop in E_x.

Crucially, there is a difference in phase between the current signals shown in Fig. 3(a). This is because, in the case where the WS-DL decoupling occurs, the rapid transfer of electrons from one reservoir to the other (for example from left to right) allows the system to approach electrostatic equilibrium. Then, when the polarity of the driving voltage is reversed, the electrons can quickly begin to move in the opposite direction (right
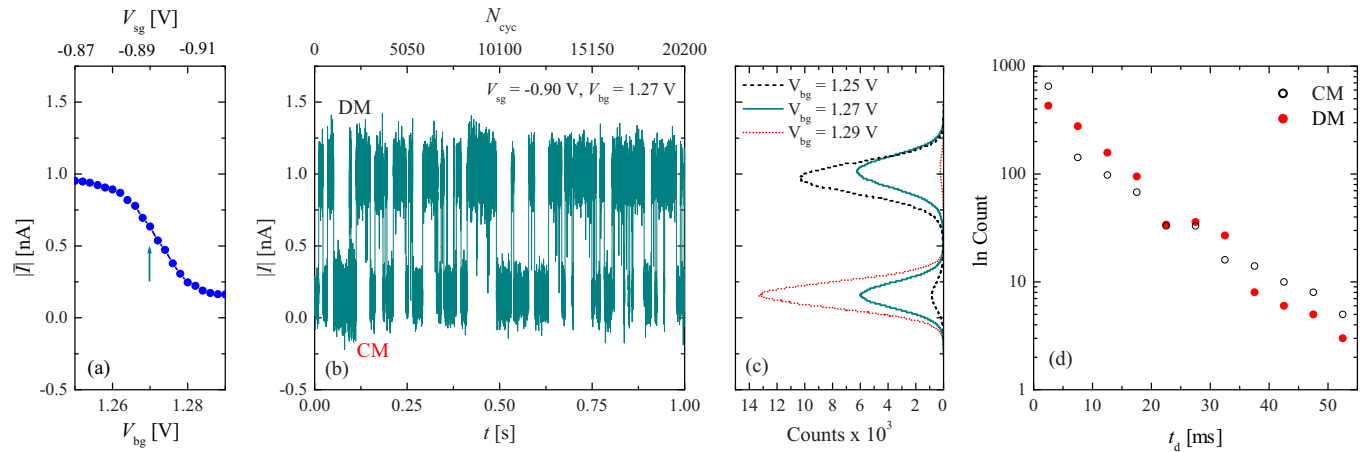
FIG. 4. (a) $|\bar{I}|$ against V_{bg} and V_{sg} close to the transition between the DM and CM regimes. The arrow indicates the point at which the time spent in the DM and CM is approximately equal. (b) $|I|$ against t for $V_{sg} = -0.9$ V and $V_{bg} = 1.27$ V. The top axis indicates the number of ac cycles. (c) Histograms for the data shown in (b) and for the cases in which the system is mostly in the DM or CM regimes, for $V_{bg} = 1.25$ and 1.29 V, respectively. The data points are binned in 10 pA intervals. (d) Distribution of the dwell times t_d recorded for each transport mode over a period of 1.8 s. The values of t_d are binned in 5 ms intervals.

to left). In the case where the decoupling does not occur during the initial half cycle, a large imbalance of charge still exists even when the polarity of the driving voltage begins to change. This charge imbalance continues to drive the electrons from left to right until the driving voltage becomes large enough to reverse the flow. Thus the behavior of the system during one half cycle directly influences the behavior during the next, which influences the behavior during the subsequent cycle, and so on. A phase difference is therefore established between the two current wave forms and the system can become "locked" in either of these "decoupling" or "coupled" transport modes (DM and CM, respectively). In the following discussion, we characterize the phase difference between the DM and CM signals by measuring the difference in the time δt at which each signal reaches the condition $E_x = 0$, as indicated in Fig. 3(b).

As V_{bg} increases, the increasing strength of coupling between the electron system and the helium results in a transition from the DM to the CM. However, when the value of V_{bg} is set close to the voltage at which the transition occurs, a spontaneous switching between the two transport modes is observed, at frequencies much lower than that of the ac drive. To study this effect we employed a lock-in amplifier to measure the first harmonic component of the current signal. Although the current response is not sinusoidal in either the DM or CM case, this measurement allows us to record large and small current signals, demodulated from the ac carrier signal, that are related to the root-mean-square amplitudes of the DM and CM current, respectively. The amplitude of this signal, denoted $|I|$, was recorded using a spectrum analyzer at an acquisition rate of $f_{aq} = 16$ kHz. We denote the time-averaged value of this signal as $|\bar{I}|$. Working at the carrier frequency of 20.2 kHz offers several advantages. Because our circuit [Fig. 1(a)] consists of a resistor and two capacitors in series, it serves as a high-pass filter. The lock-in technique essentially modulates the low-frequency signal due to the DM-CM switching to center at the carrier frequency, which is high enough to pass through the circuit, and then demodulates to recover the original transition dynamics. Also,

modulation to higher frequencies allows the minimization of the input noise of the current preamplifier [33].

In Fig. 4(a) we show the variation of $|\bar{I}|$ (averaged over 10 seconds) as V_{bg} is swept positive and V_{sg} is swept negative. By changing V_{bg} and V_{sg} simultaneously between the values shown on the upper and lower axes, the number of electron rows formed in the CM remains approximately constant, according to a previous mapping of the structural diagram of the quasi-1D electron system [28]. However, the electron density and the pressing electric field acting on the electron system change with the electrode bias values. As V_{bg} becomes more positive and V_{sg} becomes more negative, n_s and E_z increase and $|\bar{I}|$ changes smoothly from a high value to a lower value.

This smooth change is a result of the telegraph-like switching between the two conductance modes; as the WS-DL coupling increases in strength the system spends less time in the decoupling transport mode and more time in the coupled transport mode, and the average current signal smoothly decreases from a high value to a low value. At the center of the step in $|\bar{I}|$ the system spends an equal amount of time in the DM and CM. The time dependence of $|I|$ for this bias condition is shown in Fig. 4(b). The spontaneous switching between the DM and CM is observed. The time spent between switching events is typically much longer than the ac period (49.5 μs). Histograms of the current measurements are shown in Fig. 4(c). These are determined by binning the current data points in intervals of 10 pA. (Here the Gaussian distribution of $|I|$ values around the large and small values corresponding to the DM and CM results from the white noise of the current preamplifier. This is the limiting noise source in the measurement, neglecting the low-frequency switching between the DM and CM.) For $V_{bg} = 1.27$ V the distributions are of almost equal amplitude confirming that the time spent in the DM or CM is approximately equal. By increasing (decreasing) V_{bg} by 20 mV, the WS-DL coupling is strengthened (weakened) and the time spent in the CM (DM) is greatly increased.

Further analysis of this bistability is shown in Fig. 4(d). By monitoring the switching events from the DM to CM and vice versa, dwell times t_d for both modes were determined. The resolution of the measurement of t_d is $1/f_{aq}$, which is similar to the ac period. In Fig. 4(d) we plot the number of counts falling within 5 ms intervals of t_d. The probability of mode switching follows the general exponential form $P(t_d) = P(0)e^{-t_d/\tau_0}$, where $1/\tau_0$ is a constant decay rate, indicating that the probability of mode switching is the same for each ac cycle [33,34].

V. DISCUSSION

The rate at which electrons can pass through the central microchannel depends strongly on a variety of factors that change as the values of both V_{bg} or V_{sg} are varied [28]. The electron density, pressing electric field, effective channel width, strength of the lateral electrostatic confinement, and the commensurability of the electron lattice within the quasi-1D confinement are all dependent on the electrode bias values [35,36]. Each of these parameters can influence the WS-DL decoupling threshold force. The conductance of the electron system when the WS is both coupled to and decoupled from the DL, and therefore the rate at which electrons can move between the reservoirs, is also influenced by these factors. We therefore expect the WS-DL decoupling threshold to be strongly influenced by the sample bias conditions. This influence is, generally, difficult to understand quantitatively and a full analysis of the ac response of the WS in our device with changing bias conditions is beyond the scope of this report. However, it is instructive to measure the value of δt under different bias conditions and compare it with the rate of switching between the DM and CM.

In Fig. 5(b) we show the average time spent in each conductance mode $\bar{t}_d$ against the value of V_{sg}. By varying V_{bg}, each measurement was recorded at the center of the DM-CM transition [as indicated by the arrow in Fig. 4(a)] where the dwell times were approximately equal. We also show the value of δt, as recorded at V_{bg} and V_{sg} bias values close to the DM-CM transition. The points in the V_{sg}-V_{bg} plane at which the DM and CM wave forms were recorded in order to determine δt are shown in Fig. 5(a). For each value of V_{sg}, the value of V_{bg} was adjusted either side of the bistable region such that no switching behavior was observed, ensuring that the system lay fully in either the DM or CM regime. The value of δt was determined using the wave forms recorded at these bias points.

There is a clear correspondence between $\bar{t}_d$ and δt, which suggests that the system can fluctuate more rapidly between the two conductance modes when the phase difference between the two current signals becomes smaller. This in turn indicates that transitions between the conductance modes occur due to decoupling at abnormally high or low threshold forces. These decoupling events occur at times later or earlier than the average, respectively, and so overcome the phase difference between the signals. For example, for the DM case, a decoupling event for which the threshold force is much higher than the average value results in a delay in the decoupling. If this delay is long enough then the decoupling does not occur at all during the ac half cycle, and the system switches to the
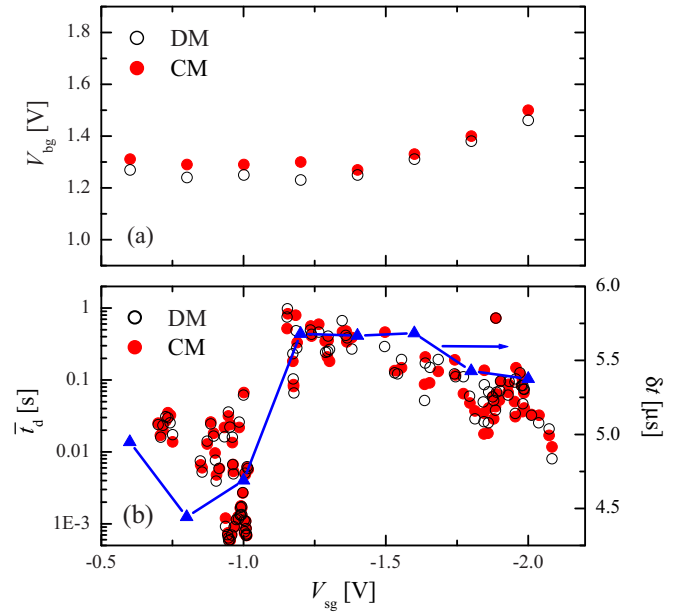

FIG. 5. (a) Values of V_{bg} at which the DM or CM wave forms were measured against V_{sg}. (b) The average dwell time $\bar{t}_d$ and δt against V_{sg}. The values of $\bar{t}_d$ for the DM and CM are approximately equal indicating that the system spends an approximately equal time in each conductance mode.

CM. Similarly, a switch from the CM to the DM can occur due to a decoupling event that occurs with a threshold force much lower than the average value.

Under this model, the switching events should become rare when threshold force values occupying the far tails of the Gaussian distribution are required to induce the transition. This is supported by the quantitative analysis shown here of both the Gaussian distribution of the decoupling threshold force and the delay between the DM and CM wave forms; the typical values of δt are several times greater than σ_t and therefore only a small fraction of the decoupling events can induce DM-CM switching. At the Gaussian tails, the quasi-exponential change of the number of decoupling events with force results in the large variation of $\bar{t}_d$ as δt changes by a small amount.

The observation of a distribution in the WS-DL decoupling threshold force is not surprising for the quasi-1D case examined here. Many experimental studies and simulations have demonstrated that geometrical confinement results in the formation of irregular quasi-1D lattice arrangements containing structural defects [36–39]. The irregular electron arrangement can impede the constructive interference that deepens the DL during BC scattering. In addition, because the defected lattice states can have many possible configurations separated by small energies, fluctuations between different lattice states occur spontaneously at finite temperature, which can also influence the DL formation. Furthermore, in our experiment the central microchannel is continuously repopulated with electrons as the current flows, and we expect the electron lattice to exhibit different configurations as it enters and moves along the microchannel. Because the DL depth depends sensitively on these factors, and the decoupling threshold force depends

on the DL depth, a distribution in the decoupling threshold is not unexpected.

External factors may, in principle, also influence the WS-DL decoupling; mechanical vibrations may lead to oscillations in the helium surface height, and so the pressing electric field exerted on the electron system, which would influence the WS-DL decoupling. More directly, the excitation of surface waves might produce an interference which reduces the depth of the DL. Electrical noise from the sample electrodes could also influence the WS-DL decoupling. However, we have found no evidence of these external factors influencing the WS-DL decoupling or the DM-CM bistability. The dilution refrigerator used in the measurement is cooled by a pulse-tube cooler, which should be the largest source of mechanical noise in our experimental setup. Upon switching off the pulse-tube cooler for short periods, during which T remains constant, no change in the decoupling behavior shown in Fig. 2 or in the values of $\bar{t}_d$ was recorded. Attempts to improve the filtering of electrical noise entering the sample cell, or to increase the noise level by adding large resistances to the dc bias lines, also resulted in no changes to the observed behavior. The spectrum of the mechanical and electrical noise exhibit maxima at certain characteristic frequencies, for example at 60 Hz in the case of the electrical noise spectrum; however, no excess switching was observed at these frequencies. We conclude that the distribution in the WS-DL decoupling threshold arises due to intrinsic structural disorder in the confined electron system and not from any external sources.

VI. TEMPERATURE AND COMMENSURABILITY DEPENDENCE OF THE TRANSPORT MODE SWITCHING

The electron motion that influences the WS-DL coupling is thermally driven, and it is therefore of obvious interest to investigate the dependence of the transport bistability on temperature. Also, it is well known that for quasi-1D WS systems the commensurability of the electron lattice with the confining potential influences the degree of electron positional order and fluctuations in electron lattice configurations [37]. When the lattice is commensurate with the confinement the system is highly ordered into rows. When the lattice is incommensurate with the confinement, structural defects appear in order to reduce the total energy of the electron system and fluctuations between metastable lattice configurations of similar energy become more common. In this case, an increase in the DM-CM switching rate should be expected.

The bistable behavior observed here can be investigated at different temperatures, and for varying degrees of lattice commensurability. However, because the average decoupling threshold depends strongly on these parameters, their variation requires that the electrode bias conditions be changed in order to remain in the bistable transport regime. As described above, the modification of the bias conditions can result in changes in many factors which influence the rate at which electrons can move between the reservoirs, and so the value of δt. In this section we demonstrate that, due to this effect, it is not straightforward to unambiguously determine the influence of temperature and commensurability on the decoupling threshold distribution.
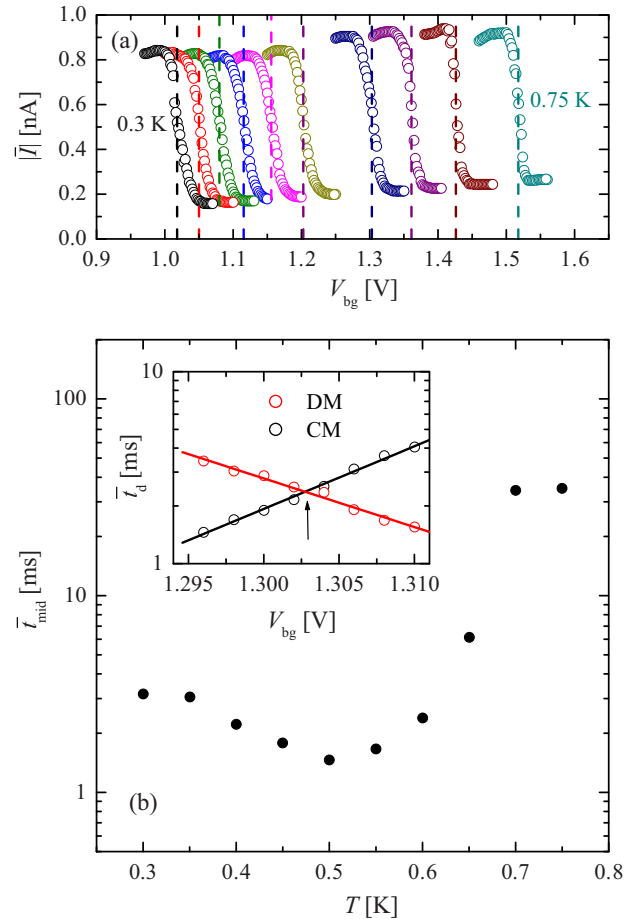

FIG. 6. (a) $|\bar{I}|$ against V_{bg} for temperatures ranging from 0.3 K to 0.75 K in 50 mK steps. The dashed lines indicate the values of V_{bg} at which $\bar{t}_{mid}$ was measured. (b) $\bar{t}_{mid}$ against T. Inset: $\bar{t}_d$ for the DM and CM against V_{bg}. The solid lines are polynomial fits to the data points. $\bar{t}_{mid}$ is defined as the value for which the polynomial functions are equal, as indicated by the arrow.

In Fig. 6(a) we show $|\bar{I}|$ against V_{bg} at different temperatures, for $V_{sg} = -0.6$ V, in the bistable transport regime. The threshold between the DM and CM regimes depends strongly on the temperature, increasing from $V_{bg} = 1.02$ V at $T = 0.3$ K to $V_{bg} = 1.52$ V at $T = 0.75$ K. This is due to the thermal motion of electrons about their lattice sites. This motion increases with temperature, degrading the structure of the dimple lattice; a higher value of V_{bg} is therefore required to maintain the coupling of the WS to the DL as the temperature increases. It is also clear that the magnitude of the current step changes with temperature as the average conductance, in both the CM and DM modes, changes with the temperature and bias conditions. The current step is smallest for $T \approx 0.5$ K, and is larger at the lowest and highest temperatures.

In Fig. 6(b) we show the average dwell time at the center of the current steps against T. Here we find the average dwell time by measuring $\bar{t}_d$ for both the CM and DM as V_{bg} is varied and, by extrapolation of the resulting data points using a polynomial line fitting, find the value for which the time spent in the decoupling and coupling modes is exactly equal. An example is shown in the inset to Fig. 6(b). As expected,

the value of V_{bg} at which this condition is satisfied is at the center of the current step, as indicated by the dashed lines in Fig. 6(a). We denote the average dwell time found by this method as $\bar{t}_{mid}$. It is clear that the value of $\bar{t}_{mid}$ exhibits a correspondence with the size of the current step. When the step size is large the dwell time is also large. This correspondence can be attributed to the dependence of δt on the difference in the relative magnitudes of the (average) conductance in the decoupling and coupled transport modes. When the difference is large, the phase difference between the current signals of the CM and DM is also large, making switching events rarer. It is not straightforward to change T and also keep δt constant. We conclude, therefore, that the changes in the bias conditions necessary to observe the DM-CM bistability as the temperature changes make it difficult to gain information about the influence of temperature on the distribution of the decoupling threshold force.

The dependence of the current bistability on the structural order of the quasi-1D lattice can be investigated by changing the gate electrode voltages in small steps in order to smoothly vary the electron density in the central microchannel. As n_s changes, so does the average number of electron rows N_y forming the quasi-1D lattice [26,36]. When the number of lattice spacings across the electron crystal is commensurate with the effective channel width, the electron system is highly ordered, forming a discrete number of rows (N_y is integer). For incommensurate cases the electron lattice becomes strongly disordered (in this case the value of N_y, calculated using our finite-element model, is noninteger) [27].

In Fig. 7(a) we show I recorded during V_{lr} ramps and for different values of V_{bg}. These measurements are similar to those shown in Fig. 2(a). Here $V_{sg} = -1$ V. The current peaks due to the WS-DL decoupling generally occur at later times as V_{bg}, and so the strength of the WS-DL coupling, increases. However, the time at which the decoupling occurs (t_p) does not increase monotonically but in a series of steps, due to the varying positional electron order as N_y changes [26]. At the center of each plateau-like feature N_y is close to integer, while each step-like change in t_p corresponds to a structural transition. N_y values calculated using FEM are shown on the plot; here N_y varies from some 14 to 18 rows. To investigate the influence of the lattice defects that are expected to proliferate at each structural transition on the WS-DL decoupling threshold, the width of each current peak was determined by fitting a Gaussian function with standard deviation σ to the current peak at each value of V_{bg}. Because the current peaks are very close to Gaussian (as shown in Fig. 2), this direct fitting procedure is a more straightforward way in which to characterize the width of the decoupling threshold force distribution than by using a model current peak in order to calculate σ_t, as was performed above. The values of σ are shown in Fig. 7(a). A dependence of σ on the positional electron order is observed; an increase in σ close to each structural transition indicates that the distribution of the WS-DL decoupling threshold increases in width, as expected.

The increase in the width of the decoupling threshold distribution close to each structural transition should result in an increased probability of switching between the DM and CM modes, and so a decrease in the dwell times $\bar{t}_d$. However, this is difficult to determine experimentally because the average
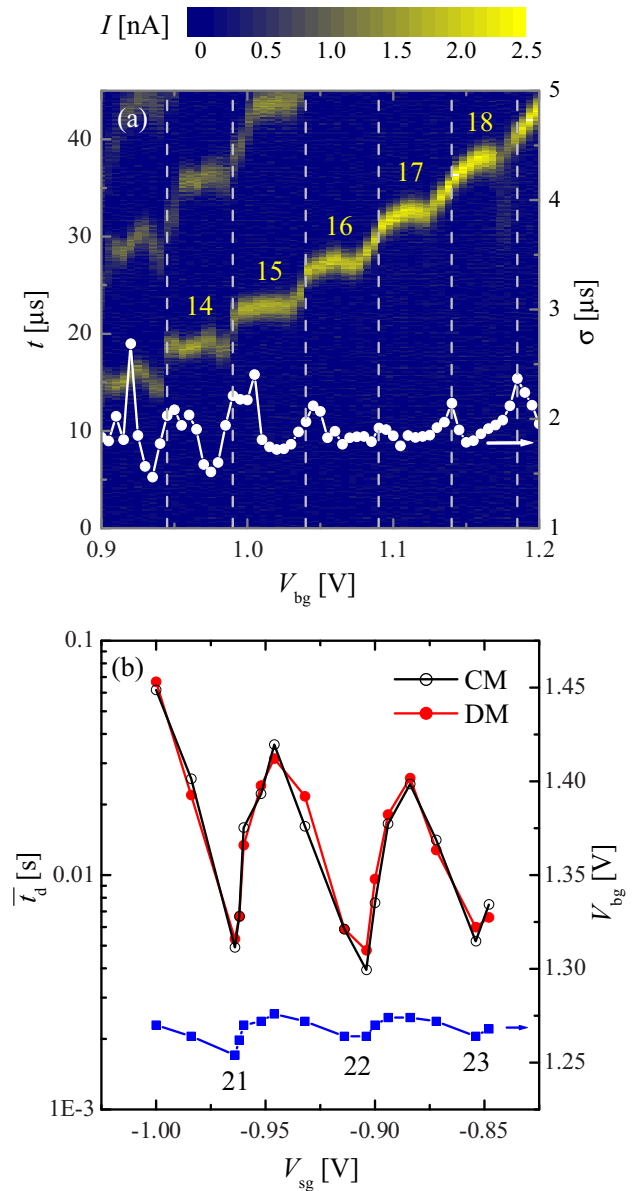

FIG. 7. (a) I against t and V_{bg}, and the standard deviation σ found by fitting a Gaussian function to the current peaks, against V_{bg}. Here $V_{sg} = -1$ V. Values of N_y obtained from FEM analysis are shown on the plot. The dashed lines are a guide to the eye, marking the points at which structural transitions between successive electron row configurations occur (N_y is half integer). (b) $\bar{t}_d$ against V_{sg} for the DM and CM. The values are measured at points close to the center of the bistable regime, which is achieved by varying V_{bg} at each value of V_{sg}. The values of V_{bg} are shown by the square symbols. N_y is close to integer at points where V_{bg} is smallest, as shown; here N_y varies from 21 to 23.

DM-CM decoupling threshold oscillates in the V_{bg}-V_{sg} plane as N_y changes. This is shown in Fig. 7(b) (square symbols), and arises due to the weakened WS-DL coupling due to positional disorder for the incommensurate lattice states. As described above, the electron transport properties are influenced by the varying bias conditions. In Fig. 7(b) we also show the variation of $\bar{t}_d$ as the bias conditions, and N_y, are changed. The value of $\bar{t}_d$ is smaller for the commensurate states. This is contrary

to the expectation that the DM-CM switching should become less frequent in this case, due to the increased order of the electron lattice. We attribute this to the influence of the WS-DL coupling strength on δt. In the DM, for commensurate states in which the average decoupling threshold force becomes larger, the decoupling occurs later in the ac cycle. This will result in a decrease in δt, and so a decrease in $\bar{t}_d$. We conclude that it is difficult to unambiguously study the influence of the lattice commensurability on the width of the decoupling threshold distribution by monitoring the DM-CM switching rate. We note that the strong influence of the lattice commensurability on $\bar{t}_d$ can also explain the scatter in the points shown in Fig. 5(b). These values were measured over a wide range of V_{bg} and V_{sg} values, with a large variation in the number of electron rows and, for each data point, the degree of commensurability.

VII. CONCLUSIONS

We have demonstrated that the decoupling of a quasi-1D electron crystal from the dimple lattice formed at the surface of liquid helium exhibits a Gaussian-like distribution in threshold force. By applying a continuous sinusoidal driving voltage to the system, a bistable regime is observed in which the system spontaneously switches between conductance modes in which decoupling does or does not occur during each ac cycle. In this regime, the switching rate between the DM and CM is extremely sensitive to the WS transport properties. We have made a quantitative analysis of the transport characteristics of the electron system, which demonstrates that the low-frequency current fluctuations are driven by decoupling events with threshold values that occupy the far tails of the Gaussian distribution. We have also shown that the low-frequency switching is exponentially sensitive to the WS transport properties. Our experiment provides an interesting example of a system in which high-frequency electron dynamics can give rise to low-frequency current fluctuations that appear in response to continuous driving. The measurement techniques demonstrated here could be useful in studying nonlinear carrier dynamics in other strongly correlated electron systems.

ACKNOWLEDGMENTS

APPENDIX

In Table I we define several abbreviations and acronyms used in the text.

TABLE I. Abbreviations and acronyms.

Abbreviation	Definition
WS	Wigner solid
DL	Dimple lattice
BC	Bragg-Cherenkov
FEM	Finite-element modeling
DM	Decoupled mode
CM	Coupled mode
T	Temperature
N_y	Number of electron rows
n_s	Average electron density
w_e	Effective electron system width
V_{gu}	Guard electrode voltage
V_{sg}	Split-gate electrode voltage
V_{bg}	Bottom-gate electrode voltage
V_{lr}	Left-reservoir electrode voltage
E_x	Electric field along the central channel
E_z	Vertical (pressing) electric field
I	Surface electron current
I_{BC}	Current under BC scattering
$|I|$	ac current magnitude
$|\bar{I}|$	Time-averaged ac current magnitude
v_r	Ripplon phase velocity
t	Time
δt	DM and CM phase difference
t_d	Conductance mode dwell time
$\bar{t}_d$	Average mode dwell time
f_{aq}	Signal analyzer acquisition frequency
σ	Gaussian standard deviation
σ_t	WS-DL decoupling time distribution standard deviation
σ_V	WS-DL decoupling voltage threshold standard deviation
σ_{E_x}	WS-DL decoupling electric field threshold standard deviation

[1] W. J. Venstra, H. J. R. Westra, and H. S. J. van der Zant, Nat. Commun. **4**, 2624 (2013).

[2] J. Atalaya, A. Isacsson, and M. I. Dykman, Phys. Rev. Lett. **106**, 227202 (2011).

[3] T. A. Fulton and L. N. Dunkleberger, Phys. Rev. B **9**, 4760 (1974).

[4] G. Gabrielse, H. Dehmelt, and W. Kells, Phys. Rev. Lett. **54**, 537 (1985).

[5] T. Walker, D. Sesko, and C. Wieman, Phys. Rev. Lett. **64**, 408 (1990).

[6] I. Mahboob, C. Froitier, and H. Yamaguchi, Appl. Phys. Lett. **96**, 213103 (2010).

[7] I. Siddiqi, R. Vijay, F. Pierre, C. M. Wilson, L. Frunzio, M. Metcalfe, C. Rigetti, R. J. Schoelkopf, M. H. Devoret, D. Vion, and D. Esteve, Phys. Rev. Lett. **94**, 027005 (2005).

[8] L. J. Lapidus, D. Enzer, and G. Gabrielse, Phys. Rev. Lett. **83**, 899 (1999).

[9] M. I. Dykman, Phys. Rev. E **75**, 011101 (2007).

[10] E. Y. Andrei (ed.), *Two-Dimensional Electron Systems on Helium and Other Cryogenic Substrates* (Kluwer Academic, Dordrecht, 1997).

[11] Y. P. Monarkha and K. Kono, *Two-Dimensional Coulomb Liquids and Solids* (Springer-Verlag, Berlin, 2004).

[12] E. Wigner, Trans. Faraday Soc. **34**, 678 (1938).

[13] C. C. Grimes and G. Adams, Phys. Rev. Lett. **42**, 795 (1979).

[14] G. A. Csáthy, D. C. Tsui, L. N. Pfeiffer, and K. W. West, Phys. Rev. Lett. **98**, 066805 (2007).

[15] C. C. Grimes and G. Adams, Phys. Rev. Lett. **36**, 145 (1976).

[16] P. Glasson, V. Dotsenko, P. Fozooni, M. J. Lea, W. Bailey, G. Papageorgiou, S. E. Andresen, and A. Kristensen, Phys. Rev. Lett. **87**, 176802 (2001).

[17] D. G. Rees, I. Kuroda, C. A. Marrache-Kikuchi, M. Höfer, P. Leiderer, and K. Kono, Phys. Rev. Lett. **106**, 026803 (2011).

[18] F. R. Bradbury, M. Takita, T. M. Gurrieri, K. J. Wilkel, K. Eng, M. S. Carroll, and S. A. Lyon, Phys. Rev. Lett. **107**, 266803 (2011).

[19] Y. P. Monarkha and V. B. Shikin, Sov. Phys. JETP **41**, 710 (1975).

[20] D. S. Fisher, B. I. Halperin, and P. M. Platzman, Phys. Rev. Lett. **42**, 798 (1979).

[21] S. A. Jackson and P. M. Platzman, Phys. Rev. B **24**, 499 (1981).

[22] M. Saitoh, J. Phys. Soc. Jpn. **55**, 1311 (1986).

[23] R. Giannetta and L. Wilen, Solid State Commun. **78**, 199 (1991).

[24] K. Shirahama and K. Kono, Phys. Rev. Lett. **74**, 781 (1995); J. Low Temp. Phys. **104**, 237 (1996).

[25] A. S. Alexandrov and J. T. Devreese, *Advances in Polaron Physics* (Springer, Berlin, 2010).

[26] D. G. Rees, N. R. Beysengulov, J.-J. Lin, and K. Kono, Phys. Rev. Lett. **116**, 206801 (2016).

[27] N. R. Beysengulov, D. G. Rees, Y. Lysogorskiy, N. K. Galiullin, A. S. Vazjukov, D. A. Tayurskii, and K. Kono, J. Low Temp. Phys. **182**, 28 (2016).

[28] D. G. Rees, N. R. Beysengulov, Y. Teranishi, C.-S. Tsao, S.-S. Yeh, S.-P. Chiu, Y.-H. Lin, D. A. Tayurskii, J.-J. Lin, and K. Kono, Phys. Rev. B **94**, 045139 (2016).

[29] F. Hecht, J. Numer. Math. **20**, 251 (2012).

[30] H. Ikegami, H. Akimoto, and K. Kono, Phys. Rev. Lett. **102**, 046807 (2009).

[31] M. I. Dykman and Y. G. Rubo, Phys. Rev. Lett. **78**, 4813 (1997).

[32] K. Mima, H. Ikezi, and A. Hasegawa, Phys. Rev. B **14**, 3953 (1976).

[33] S.-S. Yeh, W.-Y. Chang, and J.-J. Lin, Sci. Adv. **3**, e1700135 (2017).

[34] T. Grasser, Microelectron. Reliab. **52**, 39 (2012).

[35] H. Ikegami, H. Akimoto, and K. Kono, Phys. Rev. B **82**, 201104 (2010).

[36] H. Ikegami, H. Akimoto, D. G. Rees, and K. Kono, Phys. Rev. Lett. **109**, 236802 (2012); H. Ikegami, H. Akimoto, and K. Kono, J. Low Temp. Phys. **179**, 251 (2015).

[37] G. Piacente, I. V. Schweigert, J. J. Betouras, and F. M. Peeters, Phys. Rev. B **69**, 045324 (2004).

[38] A. D. Klironomos and J. S. Meyer, Phys. Rev. B **84**, 024117 (2011).

[39] K.-A. Liu and L. I, Phys. Rev. E **82**, 041504 (2010).